Adaptive Sub-band Bandwidth-Enabled Spectrum Allocation for Terahertz Communication Systems

Akram Shafie[†], Nan Yang[†], Sheeraz Alvi[†], Chong Han[‡], Salman Durrani[†], and Josep M. Jornet[§]
[†]School of Engineering, Australian National University, Canberra, ACT 2601, Australia
[‡]UM-SJTU Joint Institute, Shanghai Jiao Tong University, Shanghai, 200240, China
[§]Electrical and Computer Engineering, Northeastern University, Boston, MA 02120, USA
Emails: akram.shafie@anu.edu.au, nan.yang@anu.edu.au, sheeraz.alvi@anu.edu.au,
chong.han@sjtu.edu.cn, salman.durrani@anu.edu.au, jmjornet@northeastern.edu

ICC 2022 - IEEE International Conference on Communications | 978-1-5386-8347-7/22/$31.00 ©2022 IEEE | DOI: 10.1109/ICC45855.2022.9838818

***Abstract*—We propose a new spectrum allocation strategy for terahertz (THz) band communication (THzCom) systems. Specifically, we design multi-band-based spectrum allocation with adaptive sub-band bandwidth (ASB), by allowing to divide the spectrum of interest into sub-bands with unequal bandwidths. Due to the frequency and distance-dependent nature of the molecular absorption loss, the variation in this loss between the sub-bands would be very high at the THz band when equal sub-band bandwidth (ESB) is considered, as in the literature. The proposed strategy reduces this variation by allowing changes in the sub-band bandwidth, which leads to an overall improvement in the data rate performance. To study the impact of our strategy, we formulate an optimization problem, with the main focus on spectrum allocation, to determine the optimal sub-band bandwidth and transmit power. Thereafter, we propose reasonable approximations and transformations to solve the formulated problem. Aided by numerical results, we show that by enabling and optimizing ASB, a significantly higher data rate can be achieved by our strategy, compared to adopting ESB, and it is more beneficial to adopt ASB when the spectrum with the highest average molecular absorption loss within the THz transmission window is selected during spectrum allocation.**

***Index Terms*—Terahertz communication, spectrum allocation, adaptive bandwidth.**

I. Introduction

In an attempt to support the unprecedented increase in wireless data traffic that is expected to occur over the next decade, researchers from industry and academia have begun to study wireless communications in the terahertz (THz) band (0.1 THz–10 THz) for the sixth-generation (6G) and beyond systems [1]. The huge untapped bandwidths available at the THz band and the extremely short wavelengths of THz signals offer enormous potentials. Following the major breakthroughs on THz hardware technologies and standardization efforts over the past decade, it is envisioned that THz band communication (THzCom) systems will become a reality in the near future [2].

The exploration of novel and efficient spectrum allocation strategies is of paramount importance to exploit the potentials of the THz band [2, 3]. When such strategies are to be devised, the distinctive propagation characteristics at the THz band pose new challenges that have never been seen at lower frequencies [4]. Specifically, in addition to the severe spreading loss, the THz band is characterized by the unique frequency and distance-dependent molecular absorption loss. The molecular absorption loss introduces drastically varying path loss within the THz band and this variation increases further as the transmission distance increases. Thus, the design of novel, low-complexity, and efficient spectrum allocation strategies is of utmost significance to develop ready-to-use THzCom systems.

Multi-band-based spectrum allocation is envisioned as one of the promising solutions to support micro- and macro-scale THzCom systems, due to its ability to efficiently allocate spectral resources when the molecular absorption loss variation among the links in multiuser systems is very high [5, 6]. In these schemes, the spectrum of interest is divided into a set of non-overlapping sub-bands, and these sub-bands are exploited to serve the users in the system. The multi-band-based spectrum allocation and its performance under distance-varying usable bandwidth and interference was first discussed in [5]. A distance-aware multi-carrier (DAMC) based spectrum allocation was proposed in [6] to improve the throughput fairness among users in multiuser THzCom systems. In [6], it was proposed to assign the sub-bands with high molecular absorption coefficients to the users with longer distances and the sub-bands with low molecular absorption coefficients to the users with shorter distances, in order to take advantage of the frequency and distance-dependent nature of THz channels. By adopting DAMC-based spectrum allocation, a spectrum allocation problem in the THz band backhaul network was addressed in [7]. Furthermore, the coverage problem and the achievable data rate performance of THzCom networks when multi-band-based spectrum allocation is adopted were investigated in [8].

It is noted that the studies in [5–8] considered equal sub-band bandwidth (ESB), where the spectrum of interest is divided into sub-bands with equal bandwidth. However, to improve the spectral efficiency of multi-band-based spectrum allocation, it would be beneficial to explore spectrum allocation with adaptive sub-band bandwidth (ASB), by allowing to divide the spectrum of interest into sub-bands with unequal bandwidths. Particularly, given that the molecular absorption loss varies drastically within THz transmission windows, this variation among the sub-bands would be very high when ESB is considered [5, 6]. This variation can be reduced by allowing changes in the sub-band bandwidth. This may eventually lead to an overall improvement in the data rate performance, which

motivates this work.

In this work, we study multi-band-based spectrum allocation at the THz band by exploring the benefits of dividing the spectrum of interest into sub-bands with unequal bandwidths. We focus on a scenario where a single access point (AP) supports the downlink of multiple users which demand high data rates. We assume that DAMC-based sub-band assignment is adopted. The main contributions of this work can be summarized as follows:

- We propose multi-band-based spectrum allocation with ASB to improve the spectral efficiency of THzCom systems. To study the impact of ASB, we formulate an optimization problem, with the main emphasis on spectrum allocation, to determine the optimal sub-band bandwidth and optimal transmit power.
- To analytically solve the formulated optimization problem, we propose reasonable approximations, as well as transformations, and arrive at an approximate convex problem, which can be solved efficiently by using standard convex problem solvers.
- Aided by numerical results, we show that the proposed multi-band-based spectrum allocation with ASB achieves a significantly higher throughput compared to the multi-band-based spectrum allocation with ESB, due to its enhanced ASB capability. We also show that it is more beneficial to adopt ASB when the spectrum having the highest average molecular absorption loss within the THz transmission window is selected during spectrum allocation.

II. System Model

We consider a three-dimensional (3D) indoor THzCom system where a single AP supports the downlink of I stationary users which demand high data rates. We consider that the AP is located at the center of the ceiling of the indoor environment of interest and model it to be of height h_{A}. We also consider that users are distributed uniformly in this environment and are of heights h_{U}. We denote $\mathcal{I}$ as the set of the users and further denote r_i and $d_i = \sqrt{(h_{\mathrm{A}}-h_{\mathrm{U}})^2+r_i^2}$ as the horizontal and 3D distances between the ith user and the AP, respectively [9].

A. Channel Model

The signal propagation at the THz band is determined by spreading and molecular absorption losses. Considering this, the channel transfer function is obtained as [4]

$$H(f,d) = \frac{c}{4\pi f d}\, e^{-\frac{1}{2}K(f)d}, \tag{1}$$

where c is the speed of light, f is the frequency, d is the propagation distance of interest, and $K(f)$ is the molecular absorption coefficient at f. In (1), $e^{-\frac{1}{2}K(f)d}$ represents the molecular absorption loss which is caused by the fact that oxygen molecules and water vapor absorb THz signal energies for their rotational transition energies. It is noted that in this work, we focus only on the line-of-sight (LoS) rays of THz signals since non-line-of-sight (NLoS) rays are significantly attenuated at the THz band due to high reflection and scattering losses, as well as blockages [4, 9, 10].

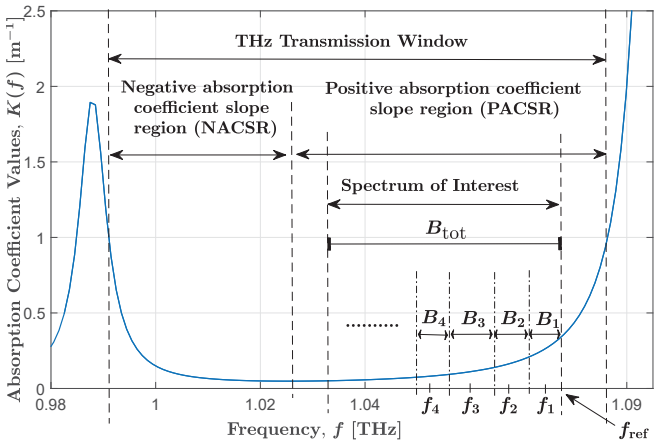

Fig. 1. Illustration of PACSR and NACSR within a THz transmission window and the arrangement of sub-bands within the PACSR.

TABLE I
AVAILABLE BANDWIDTHS WITHIN PACSRS AND NACSRS[1] [4].

PACSR		NACSR	
Frequency Range (THz)	**Bandwidth (GHz)**	**Frequency Range (THz)**	**Bandwidth (GHz)**
$0.4934 - 0.5521$	58.7	$0.5620 - 0.6107$	48.7
$0.6734 - 0.7487$	78.5	$0.6207 - 0.6515$	30.8
$0.8702 - 0.9159$	45.7	$0.7559 - 0.8513$	95.4
$1.0250 - 1.0870$	62.0	$0.9905 - 1.025$	34.5

B. THz Spectrum

We consider that the to-be-allocated spectrum of interest fully exists in either a positive absorption coefficient slope region (PACSR) or a negative absorption coefficient slope region (NACSR) of an ultra-wideband THz transmission window, as shown in Fig. 1. We note that PACSRs and NACSRs are defined as the regions within the THz transmission window where $\frac{\partial K(f)}{\partial f} > 0$ and $\frac{\partial K(f)}{\partial f} < 0$, respectively, as depicted in Fig. 1. We clarify that it is reasonable to focus on the allocation of the spectrum that exists either within a PACSR or an NACSR. This is because that the available bandwidths in each PACSR and NACSR at the THz band are in the order of tens of GHz, as shown in Table I[2]. We also note that the design principles of spectrum allocation with ASB in a PACSR are similar to those in an NACSR. Hence, without loss of generality, in the rest of the paper, we present the design principles of spectrum allocation in a PACSR, and omit the discussion of spectrum allocation in an NACSR.

We consider that the spectrum of interest is divided into S sub-bands that are of unequal bandwidths. We denote $\mathcal{S} = \{1, 2, \cdots, s, \cdots, S\}$ as the set of the sub-bands and further denote f_s and B_s as the center frequency and the bandwidth of the sth sub-band, respectively. Since ASB is considered, we have $0 \leqslant B_s \leqslant B_{\max},\ \forall s \in \mathcal{S}$, where $B_{\max}$ denotes the upper

[1]The values in Table I are calculated considering that the regions where molecular absorption coefficient values are less than one correspond to THz transmission windows [4].

[2]To fully harness the potential of the huge available bandwidths at the THz band, it would be more beneficial to focus on spectrum allocation with ASB when the spectrum of interest exists anywhere within the THz band, which will be considered in our future work.

bound on the sub-band bandwidth. For notational convenience, we consider that sub-bands in the set $\mathcal{S}$ are labeled such that $f_1 > f_2 > \cdots > f_S$, as shown in Fig. 1. Thus, we have

$$f_s = f_{\text{ref}} - \sum\nolimits_{k=1}^{s-1} B_k - B_s/2, \qquad \forall s \in \mathcal{S}, \tag{2}$$

where f_{ref} is the end-frequency of the spectrum of interest, as shown in Fig. 1. We then denote B_{tot} as the total available bandwidth within the spectrum of interest. Considering this, we obtain

$$\sum\nolimits_{s\in\mathcal{S}} B_s = B_{\text{tot}}. \tag{3}$$

Following [5, 6, 8], we assume that the users in the system are served by separate sub-bands. This assumption ensures intra-band interference-free data transmission, thereby eliminating the hardware complexity and the signal processing overhead caused by frequency reuse in the system. Under this assumption, we set the number of sub-bands to be equal to the number of users in the system, i.e., $S = I$. Also, following [5–7, 11], we adopt DAMC-based sub-band assignment to improve the throughput fairness among users in the THzCom system. The principle of the DAMC-based sub-band assignment is that the sub-bands with low absorption coefficients are assigned to the users with longer distances, while the sub-bands with high absorption coefficients are assigned the users with shorter distances. In our considered spectrum of interest within a PACSR, we have $K(f_s) > K(f_{s+1})$, $\forall s \in \mathcal{S}$. Considering this, in order to assign sub-bands to users as per the DAMC-principle, we assign the sth sub-band to the user that has the sth smallest distance, among all the users in the set $\mathcal{I}$.

C. Achievable Data Rate

The achievable data rate of the user assigned to sub-band s is obtained as [4]

$$R_s = B_s \log_2\left(1 + \frac{P_s G_{\text{A}} G_{\text{U}} |\alpha_s|^2}{N_0 B_s}\right), \qquad \forall s \in \mathcal{S}, \tag{4}$$

where P_s is the transmit power allocated by the AP to the user assigned to sub-band s, G_{A} and G_{U} are the antenna gains at the AP and users, respectively, and N_0 is the noise power density. Also, $|\alpha_s|^2$ is the path gain of the user assigned to sub-band s, which is given by

$$\begin{aligned} |\alpha_s|^2 &= T_s \int_{f_s - \frac{B_s}{2}}^{f_s + \frac{B_s}{2}} |H(f, d_s)|^2 \mathrm{d}f, \\ &= T_s \int_{f_{\text{ref}} - \sum_{k=1}^{s} B_k}^{f_{\text{ref}} - \sum_{k=1}^{s-1} B_k} |H(f, d_s)|^2 \mathrm{d}f, \quad \forall s \in \mathcal{S}, \end{aligned} \tag{5}$$

where T_s is the duration of the pulse transmitted in sub-band s [8]. Finally, we clarify that the inter-band interference (IBI) is not considered in this work due to the fact that recent studies have proposed IBI suppression schemes that can suppress IBI with minimal throughput degradation and waveform designs that minimize power leakages to adjacent bands [11, 12].

III. Optimal Spectrum Allocation

It is of utmost importance to design novel and efficient spectrum allocation strategies to harness the potential of huge available bandwidths at the THz band. With this in mind, we study spectrum allocation with ASB for the considered multiuser THzCom system. Particularly, we aim to maximize the achievable data rate under given sub-band bandwidth and power constraints. Mathematically, the problem is formulated as

$$\begin{aligned} \mathbf{P^o}: \quad & \underset{P_s, B_s, \forall s\in\mathcal{S}}{\text{maximize}} \quad \mathcal{E}(R_1, R_2, \cdots, R_S) && \text{(6a)} \\ & \text{subject to} \quad \sum\nolimits_{s\in\mathcal{S}} P_s \leqslant P_{\text{tot}}, && \text{(6b)} \\ & \qquad\qquad 0 \leqslant P_s \leqslant P_s^{\max}, \qquad \forall s \in \mathcal{S}, && \text{(6c)} \\ & \qquad\qquad \sum\nolimits_{s\in\mathcal{S}} B_s = B_{\text{tot}}, && \text{(6d)} \\ & \qquad\qquad 0 \leqslant B_s \leqslant B_{\max}, \qquad \forall s \in \mathcal{S}. && \text{(6e)} \end{aligned}$$

In this work, we aim to maximize the minimum data rate among all users, which has also been adopted by some previous relevant studies, e.g., [6, 8]. Therefore, $\mathcal{E}(R_1, R_2, \cdots, R_s) = \min_{s\in\mathcal{S}}\{R_s\}$. Moreover, (6b) reflects the power budget at the AP and (6c) ensures that the power allocated to user is upper bounded by $P_s^{\max}$. Furthermore, the justifications of (6d) and (6e) are given in Section II-B.

A. Solution Approach

We now present the solution adopted to solve the formulated optimization problem $\mathbf{P^o}$. We note that it is challenging to directly solve $\mathbf{P^o}$ due to the difficulty in obtaining the data rate, R_s, in the objective function of $\mathbf{P^o}$. Specifically, it is necessary to find the path gain, $|\alpha_s|^2$, to obtain R_s. However, on one hand, obtaining $|\alpha_s|^2$ as per (5) involves an integral and the limits of the integral depend on the design variables B_k, $\forall\ k \in \mathcal{S}$. On the other hand, the values of $K(f)$ for all frequencies within the spectrum of interest are required to obtain $|\alpha_s|^2$. Although $K(f)$ for all frequencies within the spectrum of interest can be found using the methodology in [4] with the aid of HITRAN database values, there does not exist a tractable expression that maps f to $K(f)$. This implies that it is extremely difficult, if not impossible, to analytically solve $\mathbf{P^o}$ using the traditional optimization theory techniques [13]. To overcome this challenge, we make two assumptions which enable us to obtain $|\alpha_s|^2$ using a tractable expression of the design variables B_k, $\forall\ k \in \mathcal{S}$. We next present these assumptions as follows:

First, we overcome the obstacle caused by obtaining $|\alpha_s|^2$ as in (5) using an integral. We observe that although the molecular absorption coefficient is frequency-dependent, its variation within sub-bands are relative small when sub-bands exist within THz transmission windows. Considering this, for tractable analysis, we represent $|\alpha_s|^2$ assuming that the molecular absorption coefficient remains unchanged within each sub-band. This consideration enables us to obtain $|\alpha_s|^2$ as

$$|\alpha_s|^2 = \frac{\varrho}{f_s^2 d_s^2} e^{-K(f_s) d_s}, \tag{7}$$

where $\varrho \triangleq \left(\frac{c}{4\pi}\right)^2$. We clarify that the assumption that the molecular absorption coefficient remains unchanged within the bandwidth of interest has been adopted in previous THz band studies for tractable system design when the sub-bands have a relatively small bandwidth such as [6, 9, 14].

Second, we tackle the intractability caused by the lack of tractable expression for $K(f)$. To this end, we first obtain the values of $K(f)$ for all the values of f in the spectrum of interest using the HITRAN database and observe its variation within the spectrum of interest. We notice that the variation of $K(f)$ in the spectra that exist within PACSRs generally exhibits the behavior of an exponential function of f (see Fig. 1). Therefore, through curve fitting, we model $K(f)$ in the spectrum of interest using an exponential function of f, given by

$$\hat{K}(f) = e^{\sigma_1+\sigma_2 f} + \sigma_3, \tag{8}$$

where $\hat{K}(f)$ is the approximated molecular absorption coefficient at f and $\{\sigma_1, \sigma_2, \sigma_3\}$ are the model parameters obtained for the spectrum of interest. We note that the values of $\hat{K}(f)$ in other spectra that exist within PACSRs can also be modeled using exponential functions of f. However, the model parameters would differ from one PACSR to another.

We next substitute (2) and (8) into (7) to obtain

$$|\alpha_s|^2 = \frac{\varrho\ e^{-\hat{K}(f_s)d_s}}{(f_s d_s)^2} = \frac{\varrho\ e^{-d_s[e^{\sigma_1+\sigma_2(f_s-\sum_{k\in\mathcal{S}} a_{s,k}B_k)}+\sigma_3]}}{(f_s-\sum_{k\in\mathcal{S}} a_{s,k}B_k)^2 d_s^2}, \tag{9}$$

where $a_{s,k} = 1$ if $s > k$, $a_{s,k} = \frac{1}{2}$ if $s = k$, and $a_{s,k} = 0$ otherwise.

After utilizing the aforementioned approximations, we note that the problem $\mathbf{P^o}$ is a transformed into a tractable optimization problem. However, it is non-convex in its current form. In particular, the non-convexity in $\mathbf{P^o}$ arises due to two reasons. First, R_s in the objective function in $\mathbf{P^o}$ is not differentiable at $B_s = 0$. Second, the objective function in $\mathbf{P^o}$ is non-convex w.r.t. the design variable B_ν, since R_s is not concave w.r.t. the design variable B_ν, $\forall\ \nu \in \mathcal{S}$. We next tackle this challenge as follows:

We first handle the non-differentiability of R_s at $B_s = 0$. To this end, we consider that $B_s,\ \forall s$ is lower bounded by a very small positive number. In doing so, we transform $\mathbf{P^o}$ into the following problem, given by

$$\begin{aligned}
\mathbf{P^o}(\delta):\ &\underset{P_s,B_s,\forall s}{\text{minimize}} \quad \max_{s\in\mathcal{S}}\{-R_s\} && \text{(10a)}\\
&\text{subject to} \quad \text{(6b)} - \text{(6d)},\\
&\qquad\qquad \delta \leqslant B_s \leqslant B_{\max,s}, \qquad \forall s \in \mathcal{S}, && \text{(10b)}
\end{aligned}$$

where δ is a very small positive number. We note that the optimal value of $\mathbf{P^o}(\delta)$ converges to the optimal value of $\mathbf{P^o}$ when $\delta \to 0^+$, i.e., $\lim_{\delta\to 0^+} \mathbf{P^o}(\delta) = \mathbf{P^o}$ [13].

We next handle the non-concavity of R_s w.r.t. the design variable B_ν, $\forall\ \nu\ \in\ \mathcal{S}$. For this purpose, we consider the following substitution for B_s, given by

$$B_s = \xi_s + \omega_s \log(\varsigma_s Z_s), \quad \forall s \in \mathcal{S}, \tag{11}$$

where Z_s is the new design variable in $\mathbf{P^o}(\delta)$ that would replace B_s and $\xi_s, \omega_s, \varsigma_s$ are real constants. Thereafter, substituting (11) into (4), we obtain

$$R_s = (\xi_s + \omega_s \log(\varsigma_s Z_s)) \log_2\left(1 + \frac{P_s G_{\mathrm{A}} G_{\mathrm{U}} |\bar{\alpha}_s|^2}{N_0(\xi_s + \omega_s \log(\varsigma_s Z_s))}\right), \tag{12}$$

where

$$|\bar{\alpha}_s|^2 = \varrho\ \frac{e^{-d_s[e^{\sigma_1+\sigma_2(f_s-\sum_{k\in\mathcal{S}} a_{s,k}(\xi_k+\omega_k\log(\varsigma_k Z_k)))}+\sigma_3]}}{(f_s - \sum_{k\in\mathcal{S}} a_{s,k}(\xi_k + \omega_k \log(\varsigma_k Z_k)))^2 d_s^2}. \tag{13}$$

We observe that the expression for R_s in (12) is highly non-linear w.r.t. Z_ν for $\nu \in \mathcal{S}$. However, through careful inspection, we arrive at the following Lemma.

Lemma 1: The R_s in (12) is concave w.r.t. $Z_\nu\ \forall\ s \in\ \mathcal{S}, \nu \in \mathcal{S}$ when $1/\omega_\nu\ >\ \bar{\omega}$, where $\bar{\omega}\ =\ \sigma_2\left(D\hat{K}(f_{\text{ref}})e^{D\sigma_3} - 1\right)$, $D > d_{\max}$, and $d_{\max}$ is the maximum propagation distance, i.e., $d_{\max} = \max_{s\in\mathcal{S}} d_s$ [15].

Proof: See Appendix A. ■

Following Lemma 1, we select ω_s such that

$$1/\omega_s > \bar{\omega}, \qquad \forall s \in \mathcal{S}, \tag{14}$$

to ensure the convexity of the objective function in $\mathbf{P^o}$ w.r.t. Z_ν. We clarify that for any selected combination of real values for $\xi_s, \omega_s, \varsigma_s$, the feasible region of the term $\xi_s + \omega_s \log(\varsigma_s Z_s)$ is $\mathbb{R}$, as long as $Z_s \in \mathbb{R}$. Thus, the constraint introduced on ω_s in (14), does not add any restriction on the domain of the problem $\mathbf{P^o}(\delta)$. Within this consideration in mind, we transform $\mathbf{P^o}(\delta)$ into the following equivalent problem, given by

$$\begin{aligned}
\hat{\mathbf{P}}^{\mathbf{o}}:\ &\underset{P_s,Z_s,\forall s}{\text{minimize}} \quad \max_{s\in\mathcal{S}}\{-R_s\} && \text{(15a)}\\
&\text{subject to} \quad \text{(6b)} - \text{(6c)},\\
&\qquad \prod_{s=1}^{S} Z_s^{\omega_s} - \prod_{s=1}^{S} \varsigma_s^{-\omega_s} e^{\bar{B}_{\text{tot}} - \sum_{s\in\mathcal{S}} \xi_s} \leqslant 0, && \text{(15b)}\\
&\qquad Z_{\min,s} \leqslant Z_s \leqslant Z_{\max,s}, \qquad \forall s \in \mathcal{S}, && \text{(15c)}
\end{aligned}$$

where $Z_{\min,s} = \frac{1}{\varsigma_s} e^{\frac{\delta-\xi_s}{\omega_s}}$ and $Z_{\max,s} = \frac{1}{\varsigma_s} e^{\frac{B_{\max}-\xi_s}{\omega_s}}$. We note that (15b) and (15c) are obtained by substituting (11) into (6d) and (10b), respectively. Finally, we note that after these approximations and transformations, $\hat{\mathbf{P}}^{\mathbf{o}}$ is obtained as a standard convex optimization problem. Thus, $\hat{\mathbf{P}}^{\mathbf{o}}$ can be solved efficiently by using standard convex problem solvers [13].

IV. Numerical Results

In this section, we present numerical results to illustrate the performance of the proposed multi-band-based spectrum allocation with ASB, while considering the state-of-the-art multi-band-based spectrum allocation with ESB as the benchmark [6]. The numerical results are obtained by considering a rectangular indoor environment of size 20 m $\times$ 20 m, where an AP at the center of the indoor environment serves 14 users. We consider that the 50 GHz spectrum that exists between 1.025 and 1.075 THz is used to serve the users. We use the molecular absorption coefficient values that are calculated for the standard atmosphere with 10% humidity [4]. The values

TABLE II
VALUE OF SYSTEM PARAMETERS USED IN SECTION IV.

Parameter	Symbol	Value
Heights of the AP and users	h_{A}, h_{U}	3.0 m, 1.3 m
Antenna gains	G_{A}, G_{U}	**35** dBi, **20** dBi
Noise power density	N_0	-174 dBm/Hz
Power budget	P_{tot}	-2.5 dBm
Upper bound on power per sub-band	$P_s^{\max}$	$\frac{4}{3}\frac{P_{\mathrm{tot}}}{I}$
Upper bound on sub-band bandwidth	$B_{\max}$	4.5 GHz

of the rest of the parameters used for numerical results are summarized in Table II, unless specified otherwise.

The problem $\hat{\mathbf{P}}^{\mathbf{o}}$ is implemented in AMPL, which is popular for modeling optimization problems [16]. As for the approximation of the molecular absorption coefficient values in (8), the model parameters are $\sigma_1 = -90.996$, $\sigma_2 = 8.326\times10^{-11}$, and $\sigma_3 = 0.0452$. We note that these model parameters correspond to the maximum percentage approximation error of 2.5 %. We also note that for the substitution introduced in (11) in $\hat{\mathbf{P}}^{\mathbf{o}}$, we consider $\xi_s = 5\times10^9$, $\omega_s = 5\times10^{10}$, and $\varsigma_s = 10^{-3}\ \forall\ s\in\mathcal{S}$[3].

Fig. 2 plots the aggregated multiuser data rate, $R_{\mathrm{AG}} = \sum_{s\in\mathcal{S}} R_s$, versus the power budget for the spectrum allocation schemes with ASB and ESB. Moreover, the data rate gain of adopting ASB relative to adopting ESB, R_{AG}, defined as $\Delta R_{\mathrm{AG}}\% = \frac{R_{\mathrm{AG}}|_{\mathrm{ASB}} - R_{\mathrm{AG}}|_{\mathrm{ESB}}}{R_{\mathrm{AG}}|_{\mathrm{ESB}}}\times 100$, is also plotted, where $R_{\mathrm{AG}}|_{\mathrm{ESB}}$ and $R_{\mathrm{AG}}|_{\mathrm{ASB}}$ are the aggregated multiuser data rates for spectrum allocation schemes with ASB and ESB, respectively. We first observe that the proposed spectrum allocation scheme with ASB achieves a significantly higher R_{AG} compared to spectrum allocation with ESB for different power budget levels. This is expected since, while spectrum allocation with ESB achieves a certain R_{AG}, the capability of the proposed spectrum allocation scheme with ASB to vary the sub-band bandwidths helps to further improve R_{AG}. Second, we observe that R_{AG} for spectrum allocation scheme with ASB improves when upper bound on sub-band bandwidth, $B_{\max}$, increases. This is expected since a larger $B_{\max}$ gives more room to exploit the ASB capability, which improves the R_{AG}. These observations jointly demonstrates the significance of spectrum allocation with ASB, thereby validating the benefits of our proposed spectrum allocation strategy. We also observe that as expected, R_{AG} improves for both spectrum allocation scheme with ASB and ESB when the power budget increases. Interestingly, in the higher power budget regime, the data rate gain of adopting ASB relative to adopting ESB, ΔR_{AG}, is higher.

Fig. 3 plots R_{AG} versus total bandwidth of the spectrum of interest, B_{tot}, for the spectrum allocation schemes with ASB and ESB. Also, the spectral efficiencies of the spectrum allocation schemes with ASB and ESB are plotted. We first

[3]Using $D = 10\sqrt{2}$, $f_{\mathrm{ref}} = 1.075\times10^9$, and $\hat{K}(f_{\mathrm{ref}}) = 0.2702$, we first obtain $\bar{\omega}$ as $\bar{\omega} = 5.8159\times10^{-10}$. Considering this, we then set ω_s to be $\omega_s = 0.5\times10^9$ such that the constraint (14) is satisfied. Thereafter, although it is possible to select any real values for ξ_s and ς_s, we set ξ_s and ς_s to be 5×10^9 and 10^{-3}, respectively, to ensure the domain of Z_s defined by (15c) is within the numerical operating range of AMPL.

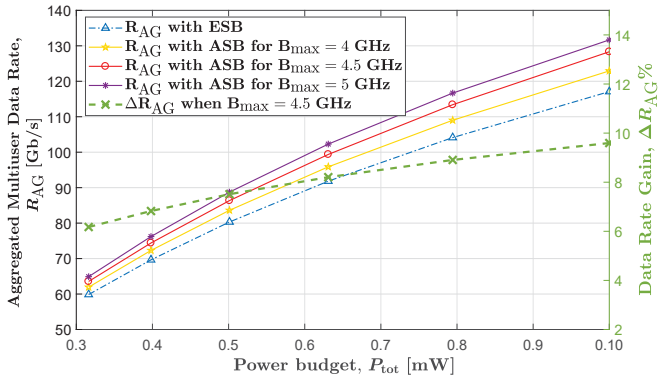

Fig. 2. Aggregated multiuser throughput versus the power budget per user.

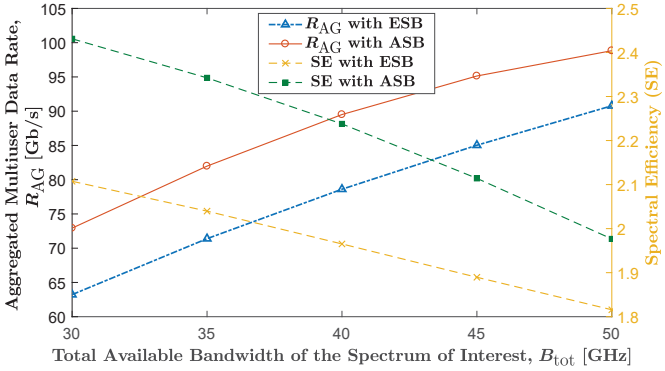

Fig. 3. Aggregated multiuser data rate and spectral efficiency versus the total available bandwidth of the spectrum of interest for different blockage densities.

observe that the spectral efficiencies of the spectrum allocation schemes with ASB and ESB decrease when B_{tot} increases. This is due to the decrease in the power density per Hz when B_{tot} increases. We next observe that R_{AG} for the spectrum allocation schemes with ASB and ESB increases when B_{tot} increases. This shows that the impact of increased availability of bandwidth for each user overwhelms the impact of decreasing spectral efficiency when B_{tot} increases.

We finally investigate the impact of molecular absorption loss on the proposed spectrum allocation scheme with ASB. To this end, we consider several 50 GHz spectra within the first THz transmission window above 1 THz, and plot the R_{AG} for the spectrum allocation schemes with ASB and ESB within these spectra versus the end-frequency of these spectra, f_{ref} in Fig. 4. Also, the average of the absorption coefficient values of the sub-bands within these spectra, $E[K_{\mathrm{abs}}]$, is plotted. We first observe that R_{AG} for the spectrum allocation schemes with ASB and ESB decreases when f_{ref} increases. This is due to the increase in $E[K_{\mathrm{abs}}]$ when f_{ref} increases, as shown in the figure, which in turn increases the molecular absorption loss in the sub-bands and reduces R_{AG}. We next observe that the data rate gain of adopting ASB relative to adopting ESB, ΔR_{AG}, increases when f_{ref} increases. This is due to the fact that, as f_{ref} increases, the molecular absorption loss variation among the sub-bands would be very high when ESB is adopted. Due to this, there is more room to improve R_{AG} by adopting ASB.

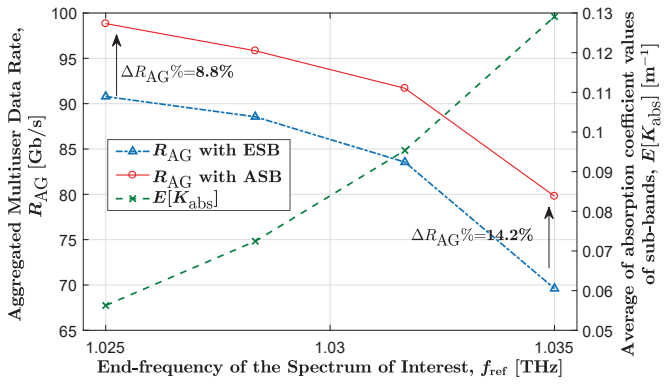

Fig. 4. Aggregated multiuser data rate versus the end-frequency of the spectrum of interest.

This observation indicates that it is more beneficial to adopt ASB when the spectrum that has the highest average molecular absorption loss is selected during spectrum allocation.

V. Conclusions

In this work, we investigated the impacts of ASB in multi-band-based spectrum allocation at the THz band. To this end, we formulated an optimization problem, with the main focus on spectrum allocation, to determine the optimal sub-band bandwidth and transmit power. We then proposed approximations and transformations to solve the formulated problem analytically. Aided by numerical results, we showed that by enabling ASB during spectrum allocation, the significantly higher throughput can be achieved as compared to adopting ESB. We also showed that it is more beneficial to adopt ASB when the spectrum having the highest average molecular absorption loss is selected during spectrum allocation.

Appendix A
Proof of Lemma 1

We prove the concavity of R_s w.r.t. to Z_ν, where $s, \nu \in \mathcal{S}$. To this end, we rearrange R_s given in (12) to obtain $R_s = B_s \log_2(1+\Upsilon_s^\nu)$, where

$$\Upsilon_s^\nu = \frac{P_s G_{\mathrm{A}} G_{\mathrm{U}}\, e^{-\Phi_{s,\nu} e^{-b_{s,\nu}\log(\varsigma_\nu Z_\nu)}}}{N_0(\Omega_{s,\nu} - b_{s,\nu}\log(\varsigma_\nu Z_\nu))^2 B_s}, \ \forall s,\nu \in \mathcal{S}, \tag{16}$$

with $\Phi_{s,\nu}{=}d_s(e^{\sigma_1+\sigma_2\Omega_{s,\nu}})$, $b_{s,\nu}{=}\sigma_2 a_{s,\nu}\omega_\nu$, and $\Omega_{s,\nu}{=}f_s - \sum_{k\in\mathcal{S}} a_{s,k}\xi_k - \sum_{k\in\mathcal{S}/\nu}\omega_k\log(\varsigma_k Z_k)$. Thereafter, we take the second derivative of R_s w.r.t. to Z_ν, while approximating the term $(\Omega_{s,\nu} - b_{s,\nu}\log(\varsigma_\nu Z_\nu))^2$ in the denominator of Υ_s^ν in (16) to be $\Omega_{s,\nu}^2$, since $\Omega_{s,\nu} \gg b_{s,\nu}\log(\varsigma_\nu Z_\nu)$. In doing so, we obtain

$$\frac{\partial^2 R_s}{\partial Z_\nu^2} = \begin{cases} E_1^{s,\nu}, & \nu < s, \\ E_2^{s,\nu} & \nu = s, \\ E_3^{s,\nu}, & \text{elsewhere}, \end{cases} \qquad \forall s\in\mathcal{S}, \nu\in\mathcal{S}, \tag{17}$$

where

$$E_1^{s,\nu} = -\left((1+\Upsilon_s^\nu)(1+b_{s,\nu}) - d_s b_{s,\nu}\ \hat{K}(f_s)e^{d_s\sigma_3}\right) B_s \times b_{s,\nu}\Upsilon_s^\nu \ln(2)^{-1} d_s\ \hat{K}(f_s)e^{d_s\sigma_3} Z_\nu^{-2}(1+\Upsilon_s^\nu)^{-2}, \tag{18}$$

$E_2^{s,\nu} = T_1 + T_2 + T_3$, and $E_3^{s,\nu} = 0$, with

$$T_1 = -\frac{\omega_s}{\ln(2)Z_s^2}\left(\log(1+\Upsilon_s^\nu) - \frac{\Upsilon_s^\nu}{(1+\Upsilon_s^\nu)}\right), \tag{19}$$

$$T_2 = -\frac{(\Upsilon_s^\nu)^2\left(b_{s,s}B_s d\ \hat{K}(f_s)e^{d_s\sigma_3} - \omega_s\right)^2}{\ln(2)\,(1+\Upsilon_s^\nu)^2 Z_s^2 B_s}, \tag{20}$$

$$T_3 = \frac{-b_{s,s}B_s\left(1{+}b_{s,s}{-}d_s b_{s,\nu}\hat{K}(f_s)e^{d_s\sigma_3}\right)d_s\hat{K}(f_s)}{\ln(2)Z_s^2\Upsilon_s^{-\nu}(1{+}\Upsilon_s^\nu)e^{-d_s\sigma_3}}. \tag{21}$$

It can be shown that $E_1^{s,\nu} < 0$ when $1/\omega_\nu > \bar{\omega}$. Also, it can be shown that $E_2^{s,\nu} < 0$ when $1/\omega_\nu > \bar{\omega}$, since $T_1 < 0$ [15, Eq. (1.512.4)], $T_2 < 0$, $\forall\ s\in\mathcal{S}, \nu\in\mathcal{S}$, and $T_3 < 0$ when $1/\omega_\nu > \bar{\omega}$ [15]. Based on these, we conclude that R_s in (12) is concave w.r.t. to Z_ν when $1/\omega_\nu > \bar{\omega}$.

References

[1] I. F. Akyildiz, A. Kak, and S. Nie, "6G and beyond: The future of wireless communications systems," *IEEE Access*, vol. 8, pp. 133 995–134 030, July 2020.

[2] M. Polese, J. M. Jornet, T. Melodia, and M. Zorzi, "Toward end-to-end, full-stack 6G terahertz networks," *IEEE Commun. Mag.*, vol. 58, no. 11, pp. 48–54, Nov. 2020.

[3] V. Petrov, T. Kurner, and I. Hosako, "IEEE 802.15.3d: First standardization efforts for sub-terahertz band communications toward 6G," *IEEE Commun. Mag.*, vol. 58, no. 11, pp. 28–33, Nov. 2020.

[4] J. M. Jornet and I. F. Akyildiz, "Channel modeling and capacity analysis for electromagnetic wireless nanonetworks in the terahertz band," *IEEE Trans. Wireless Commun.*, vol. 10, no. 10, pp. 3211–3221, Oct. 2011.

[5] C. Han, A. O. Bicen, and I. F. Akyildiz, "Multi-wideband waveform design for distance-adaptive wireless communications in the terahertz band," *IEEE Trans. Signal Process.*, vol. 64, no. 4, pp. 910–922, Feb. 2016.

[6] C. Han and I. F. Akyildiz, "Distance-aware bandwidth-adaptive resource allocation for wireless systems in the terahertz band," *IEEE Trans. THz Sci. Technol.*, vol. 6, no. 4, pp. 541–553, July 2016.

[7] X. Zhang, C. Han, and X. Wang, "Joint beamforming-power-bandwidth allocation in terahertz NOMA networks," in *Proc. Int. Conf. Sensing, Commun., Netw. (SECON)*, Boston, MA, USA, Sept. 2019, pp. 1–9.

[8] A. Moldovan, P. Karunakaran, I. F. Akyildiz, and W. H. Gerstacker, "Coverage and achievable rate analysis for indoor terahertz wireless networks," in *Proc. IEEE Int. Conf. Commun. (ICC)*, Paris, France, May 2017, pp. 1–7.

[9] A. Shafie, N. Yang, S. Durrani, X. Zhou, C. Han, and M. Juntti, "Coverage analysis for 3D terahertz communication systems," *IEEE J. Sel. Areas Commun.*, vol. 39, no. 6, pp. 1817–1832, June 2021.

[10] A. Shafie, N. Yang, and C. Han, "Multi-connectivity for indoor terahertz communication with self and dynamic blockage," in *Proc. IEEE Int. Conf. Commun. (ICC)*, Dublin, Ireland, June 2020, pp. 1–7.

[11] H. Yuan, X. Wang, K. Yang, and J. An, "Hybrid precoding for cluster-based multi-carrier beam division multiple access in terahertz wireless communications," *China Commun.*, vol. 18, no. 5, pp. 81–92, May 2021.

[12] W. Gao, Y. Chen, C. Han, and Z. Chen, "Distance-adaptive absorption peak modulation for terahertz covert communications," *IEEE Trans. Wireless Commun.*, vol. 20, no. 3, pp. 2064–2077, Nov. 2020.

[13] S. Boyd and L. Vandenberghe, *Convex Optimization*. Cambridge, U.K.: Cambridge Univ. Press, 2004.

[14] J. Sayehvand and H. Tabassum, "Interference and coverage analysis in coexisting RF and dense terahertz wireless networks," *IEEE Wireless Commun. Lett.*, vol. 9, no. 10, pp. 1738–1742, Oct. 2020.

[15] I. S. Gradshteyn and I. M. Ryzhik, *Table of Integrals, Series, and Products*, 7th ed. San Diego, CA: Academic press, 2007.

[16] R. Fourer, D. Gay, and B. Kernighan, "AMPL: A mathematical programming language," in *Algorithms and Model Formulations in Mathematical Programming. (NATO ASI Series, Series F: Computer and Systems Sciences)*, vol. 51, S. W. Wallace, Ed. Berlin, Germany: Springer, 1989.